THE JOURNAL OF PHYSICAL CHEMISTRY B

Article

pubs.acs.org/JPCB

Virial Equation of State of Water Based on Wertheim's Association Theory

Hye Min Kim,† Andrew J. Schultz,† and David A. Kofke*

Department of Chemical and Biological Engineering, 303 Furnas Hall, University at Buffalo, The State University of New York, Buffalo, New York 14260-4200, United States

ABSTRACT: Wertheim's multidensity formalism for pairwise additive molecular interaction is extended to handle nonadditive contributions and is applied to formulate an equation of state (WEOS) for the Gaussian-charge polarizable model (GCPM) of water, with cluster integrals appearing in the theory calculated via the Mayer sampling Monte Carlo method. At both sub- and supercritical temperatures, the equation of state of GCPM water obtained from WEOS converges well to Monte Carlo simulation data, and performs significantly better than the conventional virial treatment (VEOS). The critical temperature for GCPM water using a fourth-order WEOS is given to within 1.3% of the established value, compared to a 17% error shown by fifth-order VEOS; as seen in previous applications, the critical density obtained from both VEOS and WEOS significantly underestimates the true critical density for GCPM water. Examination of the magnitudes of the computed cluster diagrams at the critical density finds that negligible contributions are made by clusters in which a water molecule has both of its hydrogens involved in association interactions.

1. INTRODUCTION

The virial equation of state (VEOS) describes the pressure–volume–temperature (pVT) relation of dilute gases in terms of a power series in density with temperature-dependent coefficients known as virial coefficients:[1]

$$Z \equiv \frac{p}{pkT} = 1 + B_2\rho + B_3\rho^2 + B_4\rho^3 + B_5\rho^4 + \cdots \quad (1)$$

where Z is the compressibility factor, p is the pressure, ρ is the number density, k is the Boltzmann constant, T is the absolute temperature, and B_n is the nth virial coefficient.

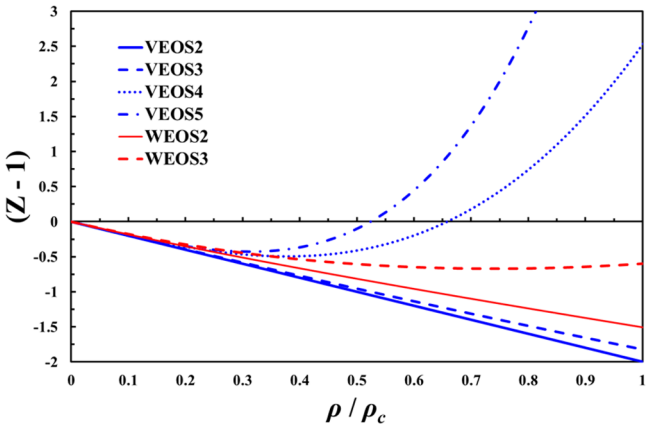

Figure 1. Convergence of VEOS for GCPM water at 650 K. Compressibility factor Z is plotted against density reduced by the critical density; ρ_c of GCPM[23] is 0.3344 g/cm^3.

B_n represents directly the interaction among n molecules and can be expressed in terms of integrals over the molecules' positions and orientations.[2] It is customary to express these integrals using cluster diagrams:[3]

$$B_2(T) = -\frac{1}{2V\Omega^2}\iint f_{12}\, dr_1\, dr_2\, d\omega_1\, d\omega_2 =$$

$$B_3(T) = -\frac{1}{3V\Omega^3}\iint f_{12}f_{13}f_{23}\, dr_1\, dr_2\, dr_3\, d\omega_1\, d\omega_2\, d\omega_3 =$$

$$B_4(T) = -\frac{1}{8V}[3 \quad +6 \quad +]$$

In these diagrams, the black lines represent the Mayer f function,

$$f_{ij} = \exp(-\beta u(r_{ij})) - 1 \quad (2)$$

where $u(r_{ij})$ is the intermolecular potential between molecule i and molecule j with separation distance r_{ij}. Each black point represents an integral of a molecule's position over all space coordinates $\mathbf{r}$ and orientations ω, normalized by Ω. The expressions above assume rigid molecules and classical behavior, although extensions to handle other cases are available.[4−6]

We have verified with several potential models that VEOS describes the thermodynamic behavior of noncondensed nonpolar fluids successfully,[4,7] converging for densities up to the spinodal and (for supercritical temperatures) beyond the critical point. However, VEOS is less effective in predicting the thermodynamic behavior of polar fluids such as water.

Received: July 7, 2012
Revised: November 10, 2012
Published: November 13, 2012

   dx.doi.org/10.1021/jp3067475 | J. Phys. Chem. B 2012, 116, 14078−14088

Benjamin et al. reported values of B_2 and B_3 in 2007 and B_4 and B_5 in 2009 for the Gaussian charge polarizable model of water (GCPM), using the overlap sampling implementation of the Mayer sampling Monte Carlo (MSMC) method.[8,9] Convergence of VEOS is demonstrated in Figure 1, which plots $Z - 1$ (i.e., the deviation from ideality) against the density. The figure shows that the VEOS4 series (i.e., VEOS truncated after $B_4\rho^3$) is converged only up to densities of about half the critical density, at which point it diverges from VEOS5. In contrast, at a comparable, slightly supercritical temperature, VEOS4 for the Lennard-Jones model is known to be converged for densities about up to the critical point.[7] For GCPM water, extending the virial series beyond VEOS5 is possible, but computing higher order virial coefficients requires much more CPU time and it is probably not worthwhile. We consider then whether an alternative molecularly detailed equation of state can be applied to describe the thermodynamic properties of associating fluids accurately.

Many equations of state for associating fluids have been developed over the years,[10−21] and although they are based on molecular concepts of association, they do not incorporate molecular-level details in a way that is done by a treatment such as the virial equation of state. Instead, they identify a few parameters that relate to general notions of molecular association, such as the size of the region available for binding, the binding strength, and the number of such binding sites, and they rely on fitting to experimental data to fix values of these parameters. Such approaches have been very successful in a variety of applications, and they are used frequently in engineering practice. Our aim in this work is different. We develop a formulation that has the character of VEOS, in that it can incorporate all available detail about the intermolecular potential, while yielding an equation of state that (unlike VEOS) is effective in describing associating systems. Such a treatment can then provide a route to truly predictive capabilities for associating systems and their mixtures, at least up to moderate densities. It may also prove valuable in interpreting the behavior of such systems.

In previous work, we examined a simple Lennard-Jones model having one or more association sites formed from a conical square-well potential and showed that the Wertheim treatment of associating fluids is much superior to the standard virial approach.[22] The Wertheim equation of state (WEOS) is derived on the basis of Wertheim's association theory[13,15] and can be used as an effective alternative to the VEOS in the respect that WEOS maintains a molecular level detail like the VEOS. We derived the WEOS for 1-site, 2-site, and 4-site association models up to the fourth order in density. WEOS showed an excellent convergence to the Monte Carlo simulation results in the NpT ensemble while the VEOS failed significantly to predict the pVT behavior of those association models.

In the present work, we examine WEOS for a much more realistic model, the Gaussian charge polarizable model (GCPM) of water due to Paricaud et al.,[23] and illustrated in Figure 1. It is well-known that water molecules associate via hydrogen bonds and that this has a profound influence on their behavior. Fixed-charge models such as TIP4P are optimized for the liquid phase, and therefore, they provide a poor description of the vapor.[24] Polarizable models such as GCPM water are needed to account for the multibody effects that make water molecules in the vapor behave differently from those in condensed water. GCPM water includes Gaussian-distributed partial charges and a dipole polarizability, and it has been shown to characterize both the liquid and the vapor phases well. Wertheim's treatment, however, is formulated for pairwise additive molecular models, and it requires some extension before it can be applied to a multibody potential such as GCPM water.

In the next section, we explain how to derive WEOS for GCPM on the basis of Wertheim's theory. In section 3, we review the Mayer sampling method used as the computational approach for evaluating the coefficients appearing in the WEOS. We present and discuss the simulation results in section 4, and we summarize our work in section 5.

2. WERTHEIM'S EQUATION OF STATE FOR GCPM WATER

2.1. Formalism and Theory. The grand-canonical partition function Ξ is given by

$$\Xi = \sum_{N=0}^{\infty} \frac{1}{N!} \int \cdots \int \exp(-\beta u_N) \cdot \prod_{i=1}^{N} z(i)\, \mathrm{d}1 \ldots \mathrm{d}N \tag{3}$$

where u_N is total intermolecular potential among N molecules and $z(i)$ is the constant fugacity. u_N is given by[25]

$$\begin{aligned} u_N &= \sum_{i<j} u_{ij} + \sum_{i<j<k} u_{ijk} + \sum_{i<j<k<l} u_{ijkl} + \cdots \\ &= \sum_{i<j} u_{ij} + \Delta u_3 + \Delta u_4 + \cdots \end{aligned} \tag{4}$$

where u_{ij} is the pairwise intermolecular potential between molecule i and j, Δu_3 is the sum of nonadditive three-body interactions, Δu_4 is the sum of nonadditive four-body interactions, and so on. Ξ can be represented diagrammatically,

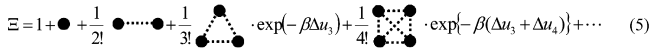

(5)

where the dotted black bonds represent $e_{ij} = \exp(-\beta u_{ij})$ and the black points are z-points.

Ξ can be re-expressed in terms of pairwise and nonpairwise terms.

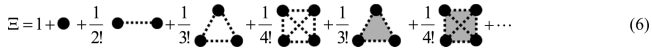

(6)

where a shaded triangle represents a 3-body f bond, such that  and likewise the diagram with the shaded square represents  . We apply to the purely pairwise terms the substitution $e_{ij} = f_{ij} + 1$, where f_{ij} is the pairwise Mayer f function and is represented by solid-line bonds,

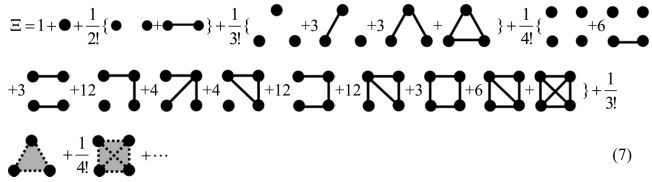

(7)

The logarithm of Ξ is a more useful form because $pV = kT \ln \Xi$, with V the volume. In eq 7, disconnected diagrams are eliminated upon application of a Taylor series expansion for the logarithm function. Consequently, ln Ξ is expressed as a sum of the connected diagrams containing f_{ij} bonds and z points:

dx.doi.org/10.1021/jp3067475 | J. Phys. Chem. B 2012, 116, 14078−14088

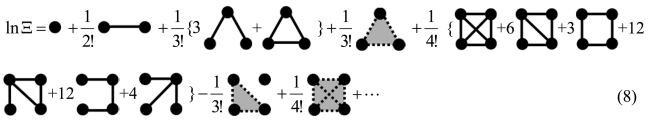

(8)

From this point, the major difference from the conventional virial development is the substitution of f_{ij} to a nonassociation part and association part.[13,15] We use a three-association-site model to represent two hydrogen sites and one oxygen site, which are labeled here as A, B, and C, respectively. The associations between A and C or B and C are allowed, but the association between A and B is not allowed. Then f_{ij} can be decomposed into a reference term (f_R) and four association terms (f_{XY}). To decompose f_{ij} bonds, we should decompose the intermolecular potential first. The intermolecular potential u_N can be decomposed as

$$u_{ij} = u_R + u_{AC} + u_{BC} + u_{CA} + u_{CB} \tag{9}$$

where u_R is a reference (nonassociation) potential and u_{XY} is an association potential between site X on molecule i and site Y on molecule j. The criteria used to separate the potential into reference and association are explained in detail in section 2.2.

With the potential decomposition in eq 9, f_{ij} is separated as

$$f_{ij} = f_R + e_R \cdot \{f_{AC} + f_{BC} + f_{CA} + f_{CB}\} \tag{10}$$

where $f_x = e^{-\beta u_x} - 1$. We exclude bonding between multiple pairs of sites on a single pair of molecules, and the result is that terms containing products such as $f_{AC}f_{CB}$ are zero and can be dropped. Equation 10 can be simplified by introducing $F_{XY} = e_R f_{XY}$:

$$f_{ij} = f_R + F_{AC} + F_{BC} + F_{CA} + F_{CB} \tag{11}$$

The e_{ij} bonds in the multibody part of $\ln \Xi$ can be handled similarly. e_{ij} is decomposed into a reference term (e_R) and several association terms.

$$\begin{aligned} e_{ij} &= e_R + e_R \cdot \{f_{AC} + f_{BC} + f_{CA} + f_{CB}\} \\ &= e_R + F_{AC} + F_{BC} + F_{CA} + F_{CB} \end{aligned} \tag{12}$$

By applying eqs 11 and 12 in eq 8, we can express $\ln \Xi$ in terms of f_R, e_R, F_{AC}, F_{BC}, F_{CA}, F_{CB}, and z points. Then $\ln \Xi$ after the bond decomposition can be used to get a total molecular density ρ by differentiation with respect to z:

$$\frac{\rho}{z} = \frac{\delta \ln \Xi}{\delta z} \tag{13}$$

Diagrammatically, the functional derivative of $\ln \Xi$ with respect to z can be obtained by enumerating all unique diagrams that can be generated by converting a field z point in the $\ln \Xi$ diagrams into a root point.[26]

In a three-association-site model, ρ is written as a sum of eight density variables:

$$\rho = \rho_0 + \rho_A + \rho_B + \rho_C + \rho_{AB} + \rho_{AC} + \rho_{BC} + \rho_{ABC} \tag{14}$$

The diagrams in each ρ_α are classified on the basis of the association bonds at the root point. For example, if the root point in a diagram has an association interaction at site A only, it is classified as part of ρ_A. If the root point in a diagram has no association interaction, that diagram is identified with the monomer density, ρ_0. If all the three association sites in a root point are bonded, that diagram is in ρ_{ABC}.

For example, ρ_0 and ρ_A are given by

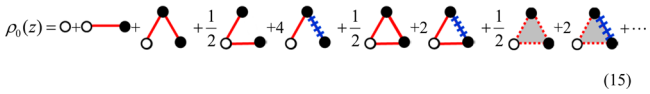

(15)

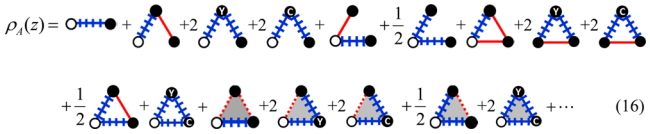

(16)

where the red solid lines represent f_R bonds, the blue hatched bonds represent one of four association bonds (F_{XY}) and the red dotted lines indicate e_R bonds (in all that follows, no e- or f-bonds appear in any diagrams (such as are in the diagrams in eq 8), so the red coloring is not essential to distinguishing the e_R- or f_R-bonds from the e- and f-bonds). The letters on the black points represent the sites participating in the corresponding association bonds. The letters X, Y, and Z represent the sites {A, B}, {A, C}, and {A, B, C} participating in the association bonds, respectively. (The letters X and Z are shown in Table 2.)

Every thermodynamic expression that we obtained so far is an expansion as a power series in z. The next step is conversion of z expansions into density expansions. In the conventional virial approach, there is only one kind of density variable, the total particle density ρ, and the conversion is straightforward. However, because we have eight density parameters in Wertheim's three-association-site model shown in eq 14, the conversion of the activity series into a density is not as obvious. Wertheim showed that the appropriate density to ascribe to each point in the converted series depends on the types of bonds that are joined to it.[15] To ensure that we correctly handle the multibody contributions, we employ a brute-force algebraic approach to the development, guided by Wertheim's prescriptions. In the base case developed by Wertheim, this approach reproduces the results he developed, while also allowing us to extend it to cases that were not addressed in his work (particularly the nonadditive contributions).

We invert the series in eq 15 to get a z expansion in terms of the monomer density ρ_0:

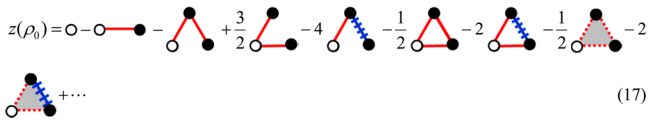

(17)

Using eq 17, every series expansion in z for the density parameters and $\ln \Xi$ can be converted into an expansion in ρ_0.

The next step is decoration of some ρ_0 into a sum of number densities, σ_α.[15] In a three-association-site Wertheim model, the σ_α factors are given by

$$\begin{aligned} \sigma_0 &= \rho_0 \\ \sigma_A &= \rho_0 + \rho_A \\ \sigma_B &= \rho_0 + \rho_B \\ \sigma_C &= \rho_0 + \rho_C \\ \sigma_{AB} &= \rho_0 + \rho_A + \rho_B + \rho_{AB} \\ \sigma_{AC} &= \rho_0 + \rho_A + \rho_C + \rho_{AC} \\ \sigma_{BC} &= \rho_0 + \rho_B + \rho_C + \rho_{BC} \\ \sigma_{ABC} &= \rho_0 + \rho_A + \rho_B + \rho_C + \rho_{AB} + \rho_{BC} + \rho_{ABC} = \rho \end{aligned} \tag{18}$$

Because sites A and site B are indistinguishable (both represent equivalent hydrogen sites), $\sigma_A = \sigma_B$ and $\sigma_{AC} = \sigma_{BC}$.

dx.doi.org/10.1021/jp3067475 | J. Phys. Chem. B 2012, 116, 14078−14088

We use each of the above to write a formula for ρ_0 that can be used to decorate the points in the expansions above:

$$\rho_0(\sigma_A) = \sigma_A - \rho_A$$
$$\rho_0(\sigma_B) = \sigma_B - \rho_B$$
$$\rho_0(\sigma_C) = \sigma_C - \rho_C$$
$$\rho_0(\sigma_{AB}) = \sigma_{AB} - \rho_A - \rho_B - \rho_{AB}$$
$$\rho_0(\sigma_{AC}) = \sigma_{AC} - \rho_A - \rho_C - \rho_{AC}$$
$$\rho_0(\sigma_{BC}) = \sigma_{BC} - \rho_B - \rho_C - \rho_{BC}$$
$$\rho_0(\sigma_{ABC}) = \sigma_{ABC} - \rho_A - \rho_B - \rho_C - \rho_{AB} - \rho_{BC} - \rho_{ABC} \quad (19)$$

If a point has associations at a set of sites α, we decorate that point with the $\rho_0(\sigma_{\Gamma-\alpha})$ function in eq 19, where Γ is the set {A, B, C}. For example, if a point has association interactions at site A and B, that point is decorated with $\rho_0(\sigma_C)$; this introduces new diagrams having articulation points, but these cancel with other diagrams, and the decorated diagram ends up simply having σ_C point in place of the ρ_0 point. In the process all singly connected diagrams are eliminated from the series and the remaining diagrams in $\ln \Xi$ have a σ_α factor for each point that depends on association bonds that are joined to it. The pressure and the densities can be expressed in terms of additive and nonadditive Wertheim cluster integrals and σ_α factors, thus

$$\begin{aligned}\beta p = \rho &- \frac{1}{2}W_{000002}\sigma_{ABC}{}^2 - 2W_{000110}\sigma_{AB}\sigma_{AC} + W_{000003}\sigma_{ABC}{}^3 + W_{000111}\sigma_{AB}\sigma_{AC}\sigma_{ABC} + W_{010110}\sigma_A\sigma_{AB}\sigma_{AC} + W_{001200}\sigma_C\sigma_{AB}{}^2 \\ &+ W_{000120}\sigma_{AB}\sigma_{AC}{}^2 + W_{000210}\sigma_{AB}{}^2\sigma_{AC} + W_{000004}\sigma_{ABC}{}^4 + W_{000112}\sigma_{AB}\sigma_{AC}\sigma_{ABC}{}^2 + W_{010111}\sigma_A\sigma_{AB}\sigma_{AC}\sigma_{ABC} + W_{000220}\sigma_{AB}{}^2\sigma_{AC}{}^2 \\ &+ W_{001201}\sigma_C\sigma_{AB}{}^2\sigma_{ABC} + W_{000121}\sigma_{AB}\sigma_{AC}{}^2\sigma_{ABC} + W_{000211}\sigma_{AB}{}^2\sigma_{AC}\sigma_{ABC} + W_{020110}\sigma_A{}^2\sigma_{AB}\sigma_{AC} + W_{011200}\sigma_A\sigma_{AB}{}^2\sigma_C \\ &+ W_{001210}\sigma_C\sigma_{AB}{}^2\sigma_{AC} + W_{010210}\sigma_A\sigma_{AB}{}^2\sigma_{AC} + W_{010120}\sigma_A\sigma_{AB}\sigma_{AC}{}^2 + W_{000130}\sigma_{AB}\sigma_{AC}{}^3 + W_{100210}\sigma_0\sigma_{AB}{}^2\sigma_{AC} + W_{000310}\sigma_{AB}{}^3\sigma_{AC} \\ &+ W_{001300}\sigma_C\sigma_{AB}{}^3 + \cdots \end{aligned} \quad (20)$$

$$\rho_A = W_{000110}\sigma_{AB} - \frac{1}{4}W_{000111}\sigma_{AB}\sigma_{ABC} - \frac{1}{4}W_{010110}\sigma_A\sigma_{AB} - \frac{1}{2}W_{000120}\sigma_{AB}\sigma_{AC} - \frac{1}{4}W_{000210}\sigma_{AB}{}^2 + \cdots \quad (21)$$

The diagrams used in density parameters such as eq 21 have a root point, unlike the diagrams used in the pressure expression (eq 20), and therefore the orders of σ points are less by one than pressure diagrams.

The coefficients W_{ijklmn} are defined in Table 2, and they represent the diagrams multiplying $\sigma_0^i\sigma_A^j\sigma_C^k\sigma_{AB}^l\sigma_{AC}^m\sigma_{ABC}^n$. Here and in all that follows, we recognize that σ_A and σ_B are equal and are both represented by σ_A; likewise σ_{AC} and σ_{BC} are represented by σ_{AC}.

2.2. Association Criteria. Implementation of the theory outlined above requires specification of the decomposition of the potential as described in eq 9. This definition should be based on considerations of whether two molecules are strongly bonded, or associated. To this end, we defined geometric and energetic criteria for hydrogen−oxygen association between two GCPM water molecules.

The geometric criteria are illustrated in Figure 2. Molecules 1 and 2 satisfy the geometric criteria for association if the separation distance r_{O-O} between the centers of their oxygen sites is between 2.1 and 3.5 Å, the angle of $O_1H_{1A}O_2$ (θ_1) is greater than 120°, and the angle between a line from H_{1A} to O_2 and a line from O_2 to the bisector of these two hydrogen sites (θ_2) is greater than 90°. These criteria were determined by short Monte Carlo simulations of two GCPM water molecules, and observing arrangements that have low energy and are appropriate for hydrogen bonding.

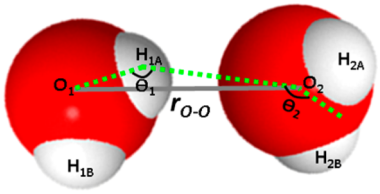

Figure 2. Geometry of GCPM water model for hydrogen−oxygen association.

The energetic criterion requires that the interaction energy of the pair of GCPM water molecules is less than −2.5 kcal/mol. This value is about half of the minimum configurational energy of water dimer in the C_s configuration reported in the literature,[23] and it is consistent with the hydrogen-bond enthalpy.[27] The fraction of orientations satisfying both the orientation and energetic association criteria when the separation criterion is satisfied is about 5%.

3. COMPUTATIONAL METHODS

3.1. Mayer Sampling. For the calculation of cluster integrals shown in VEOS and WEOS, we applied the Mayer sampling Monte Carlo (MSMC) simulation method.[28] Via Mayer sampling, the average values of the ratio of the cluster integrals of the system of interest (or *target system*) to that of an already known cluster integral (*reference system*) is calculated. In the present work, we mainly employed the overlap sampling implementation of MSMC.[29] For some diagram calculations (branch association cluster integrals shown in Table 2), we employed the direct sampling method.

In calculations of cluster integrals having only nonassociation (f_R or e_R) interactions, we employed with every configuration a flipping technique, which is a coarse orientational average. For n water molecules, 2^n configurations are generated by inverting the orientation of each water molecule about its geometric center, and the Mayer sampling integrand for those configurations are averaged. This step helps to accelerate the decay of the interactions with separation. Details of the flipping technique are described in ref 9.

In the present work, as a reference system, we used the clusters for the nth virial coefficient of hard spheres of diameter 3.2σ for the calculations of the Wertheim diagrams of order

dx.doi.org/10.1021/jp3067475 | J. Phys. Chem. B 2012, 116, 14078−14088

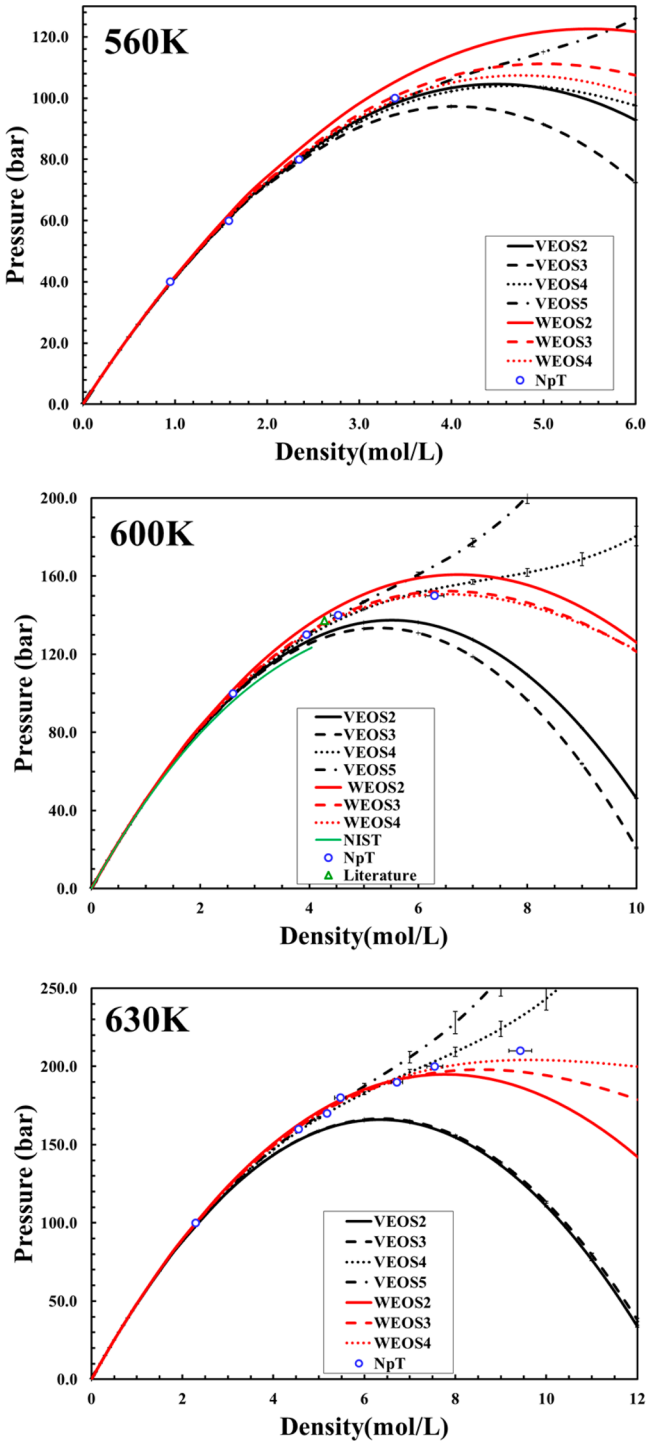

Figure 3. Pressure of GCPM water at 560, 600, and 630 K from VEOS (black lines), WEOS (red lines), *NpT* simulation (blue circle), literature[23] (green triangle), and NIST[30] (green line).

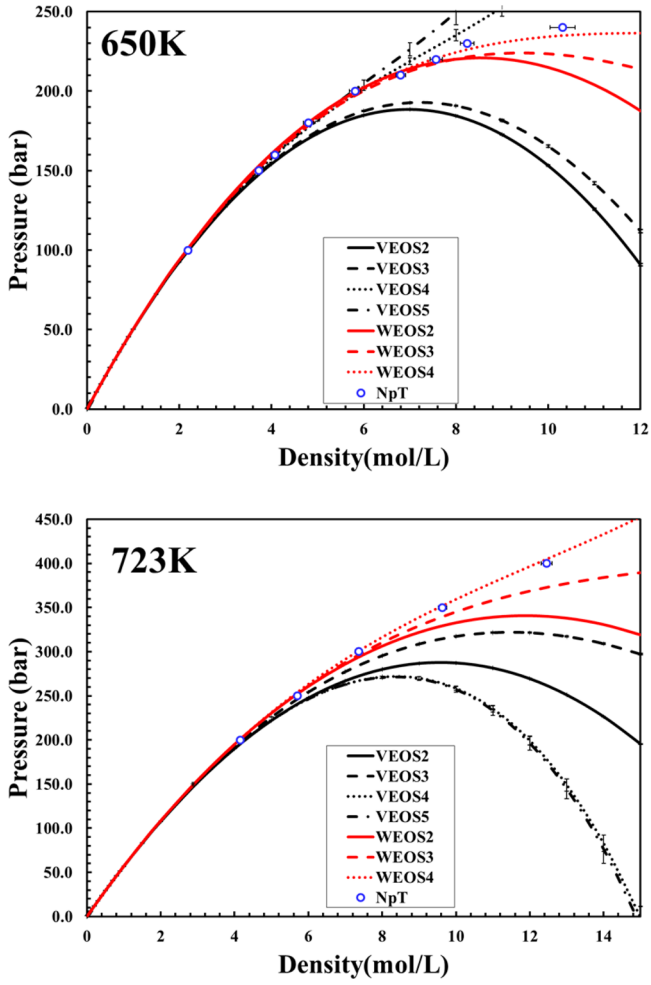

Figure 4. Pressure of GCPM water at 650 and 723 K from VEOS (black lines), WEOS (red lines), and *NpT* simulation (blue circle).

n = 2 and 3. For the calculation of the fourth-order diagrams, we used a reference system of hard spheres of diameter 5σ. For the purpose of sampling and mapping onto water configurations, each reference molecule is treated as if it were a molecule with the same geometry as GCPM water, but interacting with other reference molecules as if it were a simple hard sphere located at the geometric center of the nominal water molecule. For the calculation of diagrams having at least two adjacent F bonds, we used an associating hard-chain reference system. The system has hard association bonds, $F_{\text{hard-AC}}$, which in the reference diagram are used wherever a F bond appears in the target cluster; regular hard-sphere f-bonds are added to join other molecules to form a chain, if needed. $F_{\text{hard-AC}}$ is -1 if the distance between geometric centers of molecules 1 and 2 is between 2.1 and 3.5 Å, and the distance between site A of molecule 1 and C of molecule 2 is less than the distances between other potential bonding-site pairs; otherwise, it is zero.

The number of Wertheim diagrams involved in the pressure expansion increases rapidly with the order of EOS n. For n = 2, the number of Wertheim diagrams is 2. For n = 3, the number of diagrams is 12 (6 additive diagrams and 6 nonadditive diagrams). For n = 4, the number of diagrams is 77 (58 additive diagrams and 19 nonadditive diagrams).

We also tested using a GCPM water system as a reference instead of a hard-chain reference system. The values and the uncertainties of the Wertheim coefficients computed using a GCPM water reference are very similar with those computed using a hard-chain reference system. Therefore, we decided to use a hard-chain system as a reference in this context.

The third-order and the fourth-order terms include diagrams having rings of association bonds. We confirmed from MSMC that the contribution of these ring diagrams is almost zero, so we do not report any results including them.

dx.doi.org/10.1021/jp3067475 | J. Phys. Chem. B 2012, 116, 14078−14088

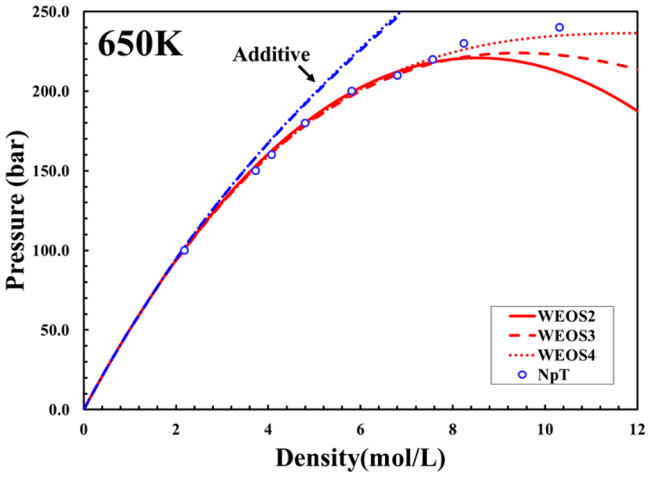

Figure 5. Pressure of GCPM water at 650 K from WEOS including additive and nonadditive contributions (red lines), WEOS including additive contributions only (blue lines, marked "additive"), and *NpT* simulation (blue circle).

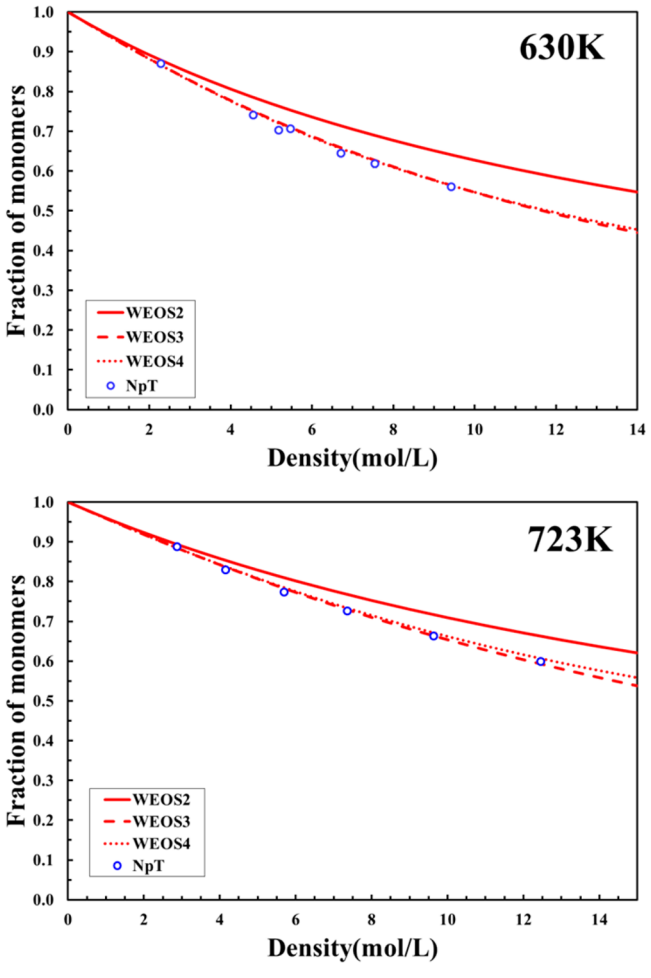

Figure 6. Fraction of monomers of GCPM water at 630 and 723 K from WEOS (red lines) and *NpT* simulation (blue circle).

3.2. *NpT* Simulation. To verify the performance of the WEOS and VEOS, we collected Monte Carlo (MC) simulation data for 256 GCPM water molecules in the isothermal–isobaric (*NpT*) ensemble. The intermolecular potential was truncated at half the length of the simulation box and thus fluctuates with the volume. We employed the same long-range correction methods as described in Paricaud et al.[23]

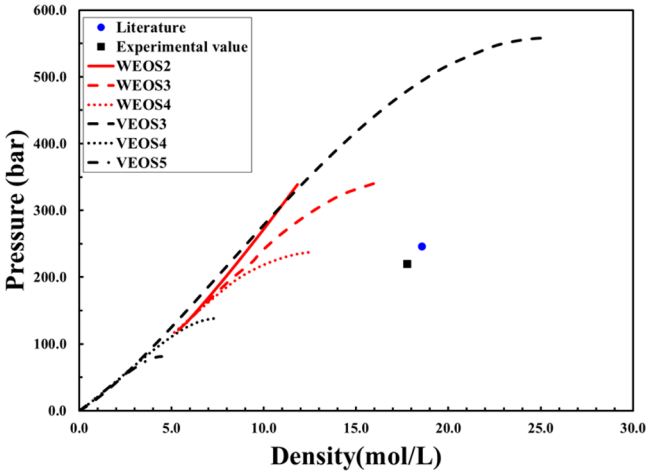

Figure 7. Spinodal curves of GCPM water from VEOS (black lines) and WEOS (red lines). The literature value[23] (blue circle) and experimental value[31] (black square) of the critical point are also presented.

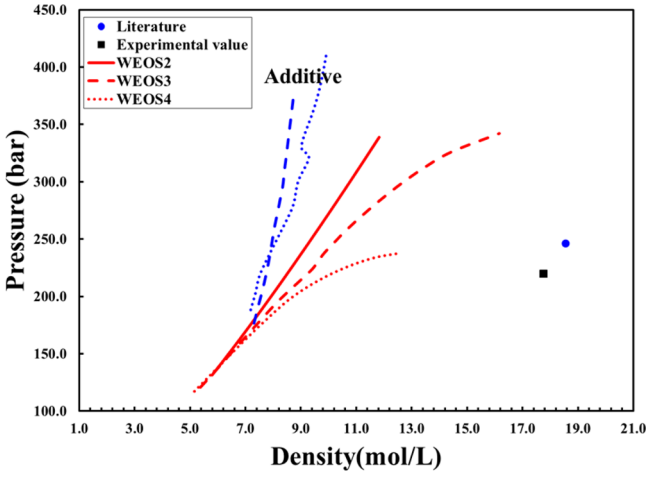

Figure 8. Spinodal curves of GCPM water from WEOS including additive and nonadditive contributions (red lines) and WEOS including additive contributions only (blue lines, labeled "additive"). The literature value[23] (blue circle) and experimental value[31] (black square) of the critical point are also presented.

Table 1. Critical Properties According to VEOS and WEOS Truncated after Various Orders *n*, for GCPM Water[a]

	$T_{c,GCPM}$ (K)	$\rho_{c,GCPM}$ (mol/L)	$P_{c,GCPM}$ (bar)
WEOS2	722	11.82	338.87
VEOS3	792	25.4	558.4
WEOS3	705	16.16	342.17
WEOS3 (additive only)	722	8.73	375.03
VEOS4	587	7.42	138.1
WEOS4	650	12.45	237.33
WEOS4 (additive only)	722	9.94	414.53
VEOS5	529	4.47	81.15
literature[23]	642	18.56	246

[a]Also tabulated are values obtained using only the additive contributions to the diagrams (i.e., excluding contributions from the non-additivity of the potential).

dx.doi.org/10.1021/jp3067475 | J. Phys. Chem. B 2012, 116, 14078–14088

Table 2. Wertheim Coefficients and Values Calculated from MSMC for GCPM Water

	group no.	σ factor	$(L/mol)^{n-1}$ 650 K	$(L/mol)^{n-1}$ 723 K
		W_{000002}	0.080423(14)	0.05706(3)
		W_{000110}	0.013907(2)	0.010437(7)
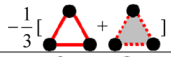	1	W_{000003}	0.0010436(14)	0.0008168(12)
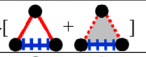	2	W_{000111}	$-8.71(12) \times 10^{-4}$	$-4.87(7) \times 10^{-4}$
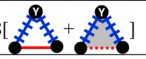	3	W_{010110}	$-1.1627(18) \times 10^{-3}$	$-5.41(2) \times 10^{-4}$
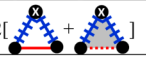	4	W_{001200}	$9.290(17) \times 10^{-5}$	$4.785(9) \times 10^{-5}$
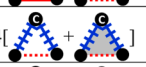	5	W_{000120}	$-3.029(7) \times 10^{-4}$	$-1.7712(17) \times 10^{-4}$
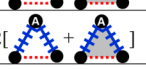	6	W_{000210}	$-5.17(5) \times 10^{-6}$	$-3.321(18) \times 10^{-6}$
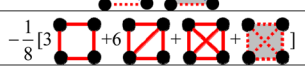	7	W_{000004}	$4.7(9) \times 10^{-6}$	$5.8(7) \times 10^{-6}$
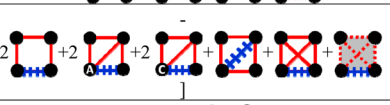	8	W_{000112}	$2.0(2) \times 10^{-5}$	$1.53(9) \times 10^{-5}$
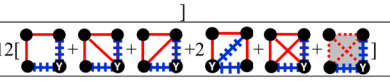	9	W_{010111}	$6(4) \times 10^{-6}$	$8.9(15) \times 10^{-6}$
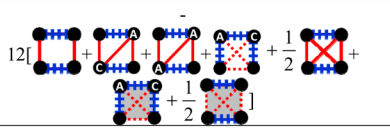	10	W_{000220}	$-1.03(18) \times 10^{-5}$	$1.1(7) \times 10^{-6}$
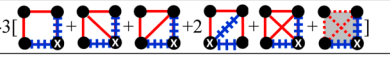	11	W_{001201}	$-7(12) \times 10^{-7}$	$4(2) \times 10^{-7}$
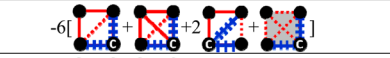	12	W_{000121}	$3.36(9) \times 10^{-5}$	$1.41(8) \times 10^{-5}$
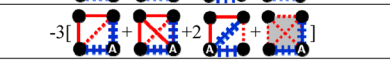	13	W_{000211}	$5.1(4) \times 10^{-6}$	$2.22(15) \times 10^{-6}$
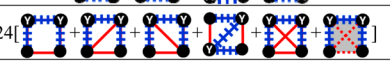	14	W_{020110}	$-7.04(3) \times 10^{-5}$	$-2.024(11) \times 10^{-5}$
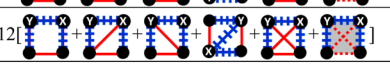	15	W_{011200}	$7.02(6) \times 10^{-6}$	$2.372(13) \times 10^{-6}$
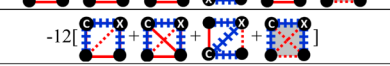	16	W_{001210}	$-8.2(4) \times 10^{-7}$	$-2.2(4) \times 10^{-7}$
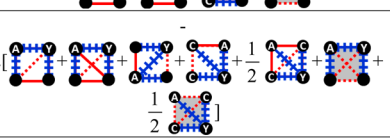	17	W_{010210}	$3.58(6) \times 10^{-6}$	$1.28(7) \times 10^{-6}$
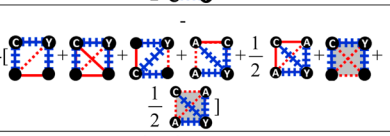	18	W_{010120}	$-2.9(6) \times 10^{-6}$	$2.3(2) \times 10^{-6}$
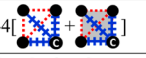	19	W_{000130}	$-5.5(3) \times 10^{-7}$	$-2.82(6) \times 10^{-7}$
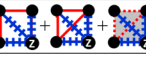	20	W_{100210}	$-6.9(3) \times 10^{-6}$	$-1.85(6) \times 10^{-6}$
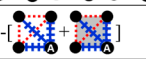	21	W_{000310}	0	0
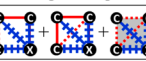	22	W_{001300}	$-2.18(10) \times 10^{-6}$	$-8.41(16) \times 10^{-7}$

The usual tail correction is applied to the exp−6 potential and the reaction field method is applied to the electrostatic potential.

We performed 10^5 MC steps for each simulation, and 17 simulations were run sequentially. The first simulation was initialized to an fcc lattice. The first two runs were regarded as the equilibration steps and discarded in the data collection. The remaining simulations were used to collect averages and error statistics. We observe that the standard deviation of the mean is less than about 3% for all averages.

dx.doi.org/10.1021/jp3067475 | J. Phys. Chem. B 2012, 116, 14078−14088

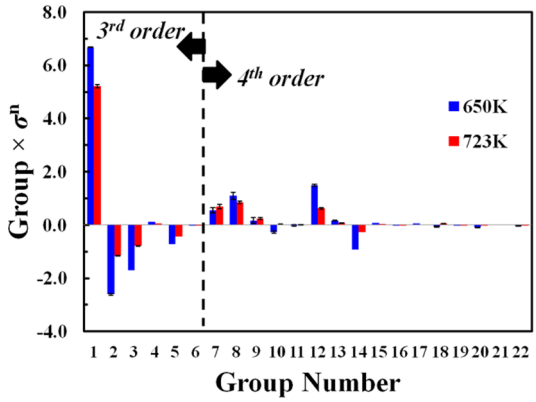

Figure 9. Third- and fourth-order diagram value multiplied by its corresponding σ factors for the critical density (18.56 mol/L) at 650 and 723 K.

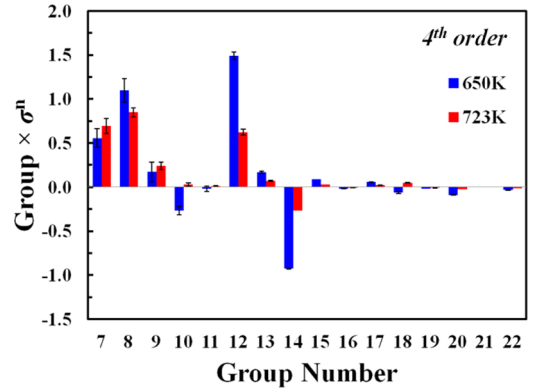

Figure 10. Fourth-order diagram value multiplied by its σ factors for the critical density (18.56 mol/L) at 650 and 723 K.

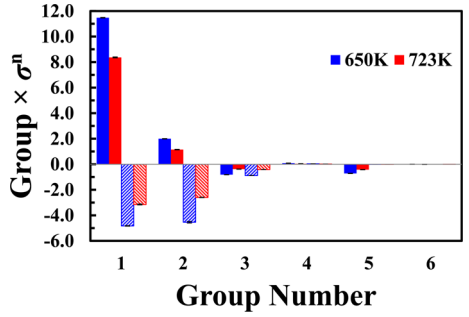

Figure 11. Third-order additive-only (solid bars) and nonadditive-only (hatched bars) diagram value multiplied by its corresponding σ factors for the critical density (18.56 mol/L) at 650 K (blue, leftmost bar in each set) and 723 K (red bar to the right of each 650 K bar).

4. RESULTS AND DISCUSSION

Figure 3 displays the pressure of GCPM water at subcritical temperatures 560, 600, and 630 K, respectively. In these plots, there are significant deviations between the different truncated VEOSs and the *NpT* simulation results. Adding higher-order contributions to the virial series does not improve the deviations among the series. In contrast, the Wertheim series shows much better convergence than all the VEOSs, and agrees very well with *NpT* ensemble simulation data. At 560 K, beyond the density about 3.4 mol/L, *NpT* simulation data are not shown because beyond that density the fluid condensed. At 630 K, *NpT* simulation results agree well with WEOS4 for

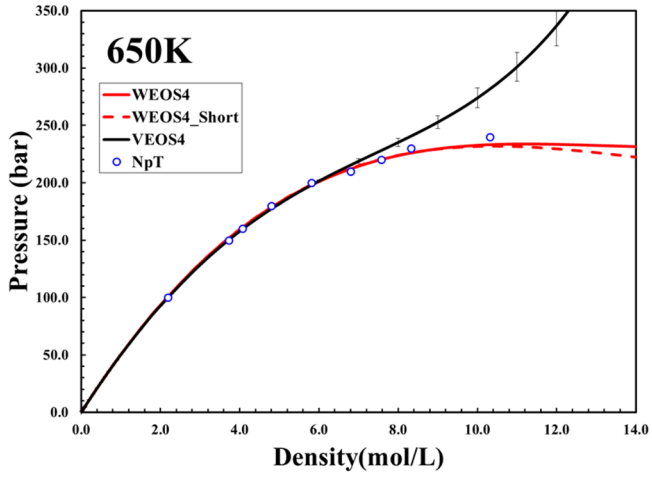

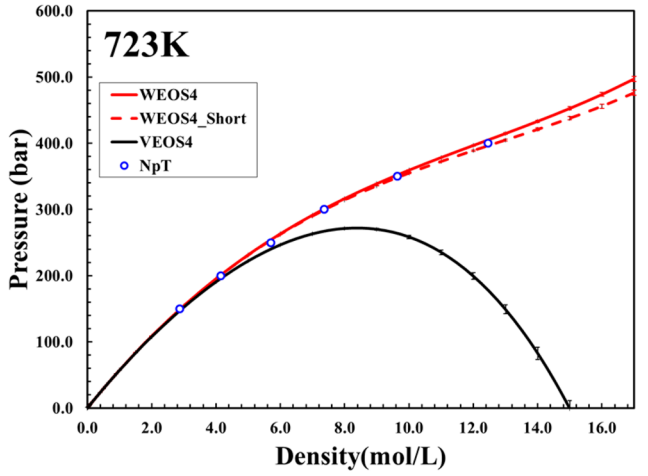

Figure 12. Pressure of GCPM water at 650 and 723 K from WEOS4 including all the diagrams (red solid line), WEOS4 including group [7, 8, 12, 14] only at fourth order (red dash line), VEOS4 (black line), and *NpT* simulation (blue circle).

densities up to about 7.5 mol/L, which according to WEOS4 is in the vicinity of the spinodal density. It appears that WEOS4 provides a good description of subcritical GCPM water over the full range of the stable vapor.

For the purpose of gauging the accuracy of the GCPM model and the WEOS characterization of it, we provide in the 600 K plot a description of real water based on an accurate equation of state from NIST.[30]

Similar improvements are observed in Figure 4 at supercritical temperatures (the critical temperature of GCPM water is 642 K[23]). At 650 K, beyond the density 4 mol/L, the virial series significantly deviate from each other and fail to describe the behavior of GCPM water, according to the *NpT* data. Again we see that the WEOS series converges up to significantly higher densities, agreeing with *NpT* simulation results up to about 8 mol/L, with WEOS4 remaining close to the *NpT* results even up to 12 mol/L. Remarkably, at all but the lowest temperatures, WEOS2 by itself performs much better than VEOS to any order examined here.

Figure 5 demonstrates the importance of the nonadditive contributions for GCPM water in computing the pressures at 650 K by comparing the pressures from WEOS including or excluding the nonadditive diagrams. The effect of the nonadditive contribution is significant.

dx.doi.org/10.1021/jp3067475 | J. Phys. Chem. B 2012, 116, 14078−14088

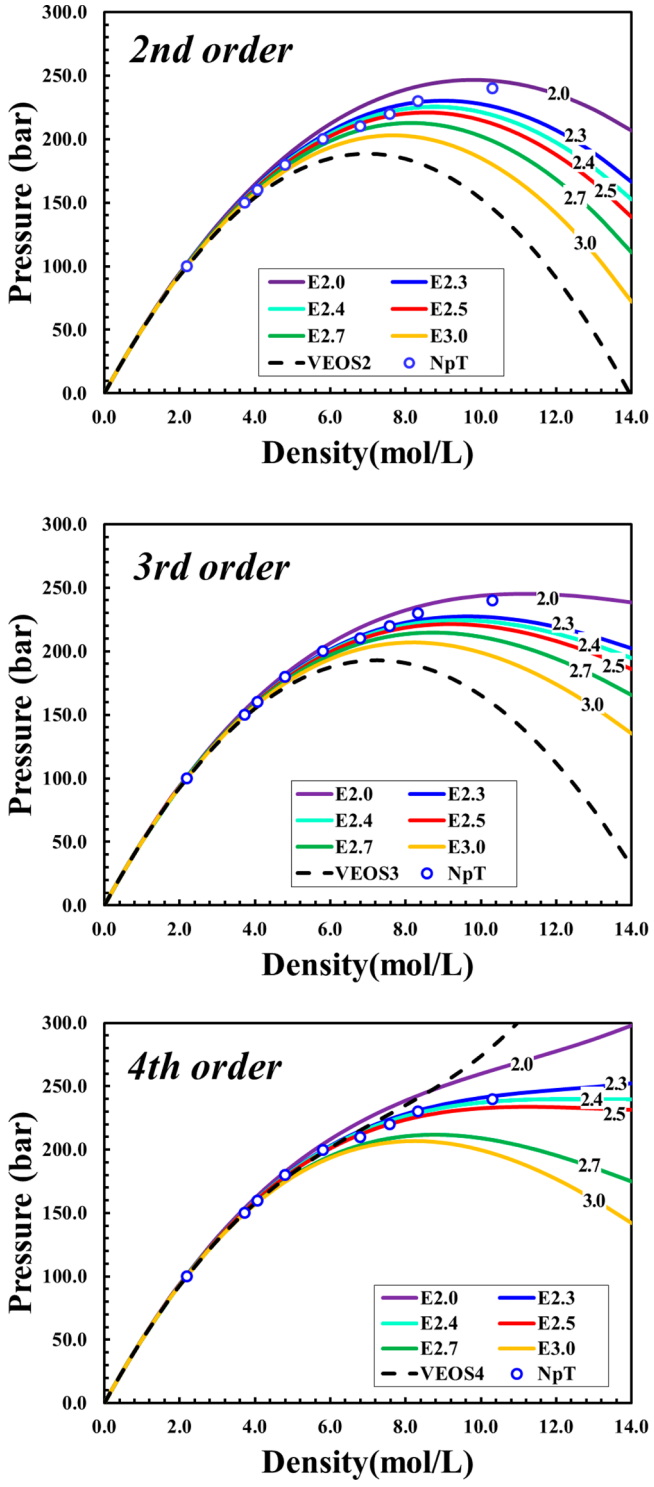

Figure 13. Pressure of GCPM water at 650 K using different energetic criterion. The energies are in units of kcal/mol.

With WEOS it is possible to calculate the different aggregation densities. For example, we plotted the fraction of monomers (ρ_0/ρ) as a function of density in Figure 6. The fraction of monomers was converged at the third order of WEOS and agreed with *NpT* very well at all temperatures. Characterizing the monomer fraction for GCPM water at various temperatures verifies WEOS as fundamentally being right.

The spinodal curve for each equation of state can be obtained from collecting the points where the first derivatives of the pressure with respect to the density are zero. Each spinodal curve ends at the critical point, which is where the second derivative of the pressure with respect to the density is also zero. In Figure 7, the spinodal curves for GCPM water are determined from VEOS and WEOS for various levels of truncation. The spinodal curves from VEOS deviate significantly from each other. The critical temperature from VEOS5 is 529 K, which is very low compared to the accepted value of 642 K for GCPM water.[23] Consistent with the quality of the pressure predictions, WEOS shows much better convergence in describing the critical properties. The critical temperature computed from WEOS4 is 650 K, which is within 1.25% of the literature value. However, as previously seen in application of density expansions to prediction of critical points (e.g., VEOS applied to nonassociating systems), the critical density given here by WEOS significantly underestimates the correct critical density for GCPM water (but it is still far better than VEOS in this application). Consistent with the discussion of the pressure for GCPM water, Figure 8 shows that the nonadditive contributions are very important in determining the spinodal curves and the critical points. Results are summarized in Table 1.

There are 6 additive Wertheim diagrams and 6 nonadditive diagrams at the third order, and 58 additive Wertheim diagrams and 19 nonadditive diagrams at the fourth order. These diagrams are grouped in Table 2 according to their σ factors, and the sum of each group is computed directly via MSMC. The group values and their uncertainties using MSMC at 650 and 723 K are listed. The red solid lines represent f_R bonds, the blue hatched bonds represent one of four association bonds (F_{XY}), the red dotted lines indicate e_R bonds and the shading indicates the diagram is multiplied by $[\exp(-\beta\Delta u_3) - 1]$ for 3 point diagrams or multiplied by $[\exp\{-\beta(\Delta u_3 + \Delta u_4)\}\text{-}1]$ for 4 point diagrams like eqs 15−17.

In Figure 9 the importance of the groups are compared by computing their contribution to the pressure at the critical density (i.e., 18.56 mol/liter), and Figure 10 expands the fourth-order data from Figure 9. For example, group 8 (W_{000112}) is associated with $\sigma_{AB}\sigma_{AC}\sigma_{ABC}^2$, and, σ_{AB}, σ_{AB}, and σ_{AB} at the critical density are 10.9117, 14.8019, and 18.56 mol/L, respectively. The diagrams showing significant contribution are the diagrams having no association bond (i.e., groups 1 and 7), the diagrams having one association bond (groups 2 and 8), the diagrams having oxygen bonded to two hydrogens on different molecules (groups 5 and 12), and the diagrams having trimers (for third-order diagrams) or tetramers, with each pair joined by singly bonded hydrogen and oxygen atoms (groups 3 and 14). The diagrams having association at both hydrogen sites are insignificant (groups 4 and 11), as are diagrams with atypical numbers of bonds: doubly bonded H sites (group 6), or triply bonded O (group 19). Figure 11 gives an indication of the size of the contributions to the groups due to diagrams that account for nonadditivity of the potential. We show this just for the third-order diagrams, and it is seen that these contributions range from half to more than double the magnitude of the additive diagrams, and usually are of the opposite sign. Similar behavior is seen in the nonadditive contributions for the fourth-order diagrams (not shown). One might consider whether a simpler WEOS can be developed by omitting those diagrams that are observed to contribute little. To this end, in Figure 12, we compare at 650 and 723 K WEOS4 including all fourth-order diagrams to WEOS4 including only groups 7, 8, 12, and 14 (WEOS4-Short). At both temperatures, WEOS4-Short is working very well and converging to the *NpT* results.

dx.doi.org/10.1021/jp3067475 | J. Phys. Chem. B 2012, 116, 14078−14088

Table 3. Wertheim Diagram Values and Uncertainties by Summing Individual Diagram Values, and Those by Computing the Diagrams as a Group

	Temperature	Individual	Group
$-\frac{1}{3}$ [+]	650K	0.001040(5)	0.0010436(14)
	723K	0.000817(9)	0.0008168(12)
-4 [+]	650K	$-8.5(2)\times10^{-4}$	$-8.71(12)\times10^{-4}$
	723K	$-4.83(11)\times10^{-4}$	$-4.87(7)\times10^{-4}$
$-\frac{1}{8}$ [3 +6 + +]	650K	$4(3)\times10^{-6}$	$4.7(9)\times10^{-6}$
	723K	$5.8(12)\times10^{-6}$	$5.8(7)\times10^{-6}$

The results in this paper use −2.5 kcal/mol as the energetic criterion for association, as we mentioned in section 2.2. In Figure 13 the sensitivity to the energetic criterion for association is examined by computing the pressures using different energetic criteria at 650 K. For all orders of truncation of the WEOS series, the pressures obtained using an energetic criterion from −2.3 to −2.5 kcal/mol are similar to each other and (at fourth order) agree with the *NpT* data over the full range of density for which data are available. If the energetic criterion is too small or large (−2.0 or −3.0 kcal/mol), WEOS does lose effectiveness in predicting the thermodynamic behavior of GCPM water. Thus we see that there is some flexibility in the choice of the definition for association for GCPM water, although the choice must provide a reasonable definition of association between water molecules.

We conclude this section by examining a detail of the computations. All diagrams within a group as defined in Table 2 multiply the same factor in the σ expansion, and thus we need compute only their sum—the values of individual diagrams are not required. Because of cancellations of diagrams within a group, it is often more efficient to compute the diagrams directly as a sum. This is demonstrated in Table 3, where the group values and their uncertainties are presented when summing individually computed diagram values, with comparison to the result obtained by computing the whole group together; results are given at 650 and 723 K. It is seen that computing the group of diagrams having same σ factors together, the uncertainty can be reduced by as much as an order of magnitude in comparison to the uncertainty of summing individual diagrams.

5. CONCLUSIONS

This work demonstrates that Wertheim's formalism—as extended here to handle multibody interactions—provides an effective foundation for the computation of the thermodynamic and structural properties of molecularly detailed associating fluids, and water in particular, for densities at least up to the critical point. The work reinforces previous observations that appropriately formulated density series are capable of identifying the liquid−vapor critical temperature and pressure, although the critical density is again significantly underestimated. We also find that magnitudes of cluster integrals can provide some insight into the type of aggregates that contribute most to the thermodynamic properties.

The VEOS is a well established model with a long history in statistical mechanics. Its primary appeal is that it provides a rigorous connection between molecular level details and macroscopic behavior. As demonstrated in this work, it is just one approach for accomplishing this, and it can prove advantageous to consider other cluster-based methods for connecting the molecular and macroscopic scales via computation of configurational integrals. Another appealing feature of VEOS is that the coefficients appearing in the equation of state can, in principle, be measured by experiment. However, in practice, it proves possible to measure only the second-order, and sometimes the third, experimentally. It would be of interest to consider whether there are ways to extract some of the WEOS coefficients from experimental data. Comparison with values computed via molecular models might provide more precise guidance on ways to improve the models.

AUTHOR INFORMATION

Corresponding Author

*E-mail: kofke@buffalo.edu. Phone: (716) 645-1173. Fax: (716) 645-3822.

Notes

The authors declare no competing financial interest.

†E-mail: H.M.K., hmkim3@buffalo.edu; A.J.S., ajs42@buffalo.edu.

ACKNOWLEDGMENTS

This work is supported by the National Science Foundation under grant CBET-0854340. Calculations were performed using resources from the University at Buffalo Center for Computational Research.

REFERENCES

(1) Mason, E. A.; Spurling, T. H. *The Virial Equation of State*; The International Encyclopedia of Physical Chemistry and Chemical Physics, Topic 10: The Fluid State, Vol. 2; Pergamon Press: New York, 1969; p 297

(2) McQuarrie, D. A. *Statistical Mechanics* **1976**, 641.

(3) Mayer, J. E.; Mayer, M. G. *Statistical mechanics*; Wiley: New York, 1940.

(4) Schultz, A. J.; Kofke, D. A. Virial coefficients of model alkanes. *J. Chem. Phys.* **2010**, *133*, 104101/1−104101/7.

(5) Caracciolo, S.; Mognetti, B. M.; Pelissetto, A. Virial coefficients and osmotic pressure in polymer solutions in good-solvent conditions. *J. Chem. Phys.* **2006**, *125*, 094903/1−094903/8.

(6) Shaul, K. R. S.; Schultz, A. J.; Kofke, D. A. Mayer-sampling Monte Carlo calculations of uniquely flexible contributions to virial coefficients. *J. Chem. Phys.* **2011**, *135*, 124101/1−124101/9.

(7) Schultz, A. J.; Kofke, D. A. Sixth, seventh and eighth virial coefficients of the Lennard-Jones model. *Mol. Phys.* **2009**, *107* (21), 2309−2318.

(8) Benjamin, K. M.; Schultz, A. J.; Kofke, D. A. Virial Coefficients of Polarizable Water: Applications to Thermodynamic Properties and Molecular Clustering. *J. Phys. Chem. C* **2007**, *111* (43), 16021−16027.

(9) Benjamin, K. M.; Schultz, A. J.; Kofke, D. A. Fourth and Fifth Virial Coefficients of Polarizable Water. *J. Phys. Chem. B* **2009**, *113* (22), 7810−7815.

(10) Heidemann, R. A.; Prausnitz, J. M. A van der Waals-type equation of state for fluids with associating molecules. *Proc. Natl. Acad. Sci. U. S. A.* **1976**, *73* (6), 1773−6.

(11) Ghonasgi, D.; Chapman, W. G. Theory and simulation for associating chain fluid. *Mol. Phys.* **1993**, *80* (1), 161−76.

(12) Chapman, W. G.; Gubbins, K. E.; Jackson, G.; Radosz, M. SAFT: equation-of-state solution model for associating fluids. *Fluid Phase Equilib.* **1989**, *52*, 31−8.

(13) Wertheim, M. S. Fluids with highly directional attractive forces. I. Statistical Thermodynamics. *J. Stat. Phys.* **1984**, *35* (1), 19−34.
(14) Wertheim, M. S. Fluids with highly directional attractive forces. II. Thermodynamic Perturbation Theory and Integral Equations. *J. Stat. Phys.* **1984**, *35* (1), 35−47.
(15) Wertheim, M. S. Fluids with highly directional attractive forces. III. Multiple Attraction Sites. *J. Stat. Phys.* **1986**, *42* (3), 459−492.
(16) Andersen, H. C. Cluster expansions for hydrogen-bonded fluids I. Molecular association in dilute gases. *J. Chem. Phys.* **1973**, *59*, 4714−25.
(17) Galindo, A.; Burton, S. J.; Jackson, G.; Visco, D. P.; Kofke, D. A. Improved models for the phase behaviour of hydrogen fluoride: chain and ring aggregates in the SAFT approach and the AEOS model. *Mol. Phys.* **2002**, *100* (14), 2241−2259.
(18) Vafaie-Sefti, M.; Modarress, H.; Meibodi, M. E.; Mousavi-Dehghani, S. A. Association equation of state for hydrogen-bonded substances. *Can. J. Chem. Eng.* **2007**, *85*, 65−74.
(19) Lencka, M.; Anderko, A. Modeling phase equilibria in mixtures containing hydrogen fluoride and halocarbons. *AIChE J.* **1993**, *39*, 533−538.
(20) Anderko, A. A simple equation of state incorporating association. *Fluid Phase Equilib.* **1989**, *45*, 39−67.
(21) Muller, E. A.; Gubbins, K. E. Molecular-based equations of state for associating fluids: A review of SAFT and related approaches. *Ind. Eng. Chem. Res.* **2001**, *40* (10), 2193−2211.
(22) Kim, H. M.; Schultz, A. J.; Kofke, D. A. Molecular Based Modeling of Associating Fluids via Calculation of Wertheim Cluster Integrals. *J. Phys. Chem. B* **2010**, *114*, 11515−11524.
(23) Paricaud, P.; Predota, M.; Chialvo, A. A.; Cummings, P. T. From dimer to condensed phases at extreme conditions: Accurate predictions of the properties of water by a Gaussian charge polarizable model. *J. Chem. Phys.* **2005**, *122*, 244511/1−244511/14.
(24) Benjamin, K. M.; Schultz, A. J.; Kofke, D. A. Gas-Phase Molecular Clustering of TIP4P and SPC/E Water Models from Higher-Order Virial Coefficients. *Ind. Eng. Chem. Res.* **2006**, *45* (16), 5566−5573.
(25) Johnson, C. H. J.; Spurling, T. H. Nonadditivity of intermolecular forces. Effects on the fourth virial coefficient. *Aust. J. Chem.* **1974**, *27*, 241−7.
(26) Hansen, J. P.; McDonald, I. R. *Theory of Simple Liquids*, 3rd ed.; Academic Press: London, 2006; 416 pp.
(27) Carey, D. M.; Korenowski, G. M. Measurement of the Raman spectrum of liquid water. *J. Chem. Phys.* **1998**, *108*, 2669−2675.
(28) Singh, J. K.; Kofke, D. A. Mayer Sampling: Calculation of Cluster Integrals using Free-Energy Perturbation Methods. *Phys. Rev. Lett.* **2004**, *92* (22), 220601/1−220601/4.
(29) Benjamin, K. M.; Singh, J. K.; Schultz, A. J.; Kofke, D. A. Higher-Order Virial Coefficients of Water Models. *J. Phys. Chem. B* **2007**, *111* (39), 11463−11473.
(30) Lemmon, E. W.; McLinden, M. O.; Friend, D. G. Thermophysical Properties of Fluid Systems. In *NIST Chemistry WebBook*; Linstrom, P. J., Mallard, W. G., Eds.; NIST Standard Reference Database Number 69; NIST: Gaithersburg, MD, http://webbook.nist.gov/chemistry/fluid.
(31) Harvey, A. H.; Peskin, A. P.; Klein, S. A. *NIST/ASME Steam Program*; Standard Reference Database 10, version 2.2; NIST: Gaithersburg, MD, 1996.